ELSEVIER

Biophysical Chemistry 89 (2001) 105–117

Biophysical Chemistry

www.elsevier.nl/locate/bpc

Short-strong hydrogen bonds and a low barrier transition state for the proton transfer reaction in RNase A catalysis: a quantum chemical study

S. Vishveshwara[a,*], M.S. Madhusudhan[a], Jacob.V. Maizel Jr[b]

[a] *Molecular Biophysics Unit, Indian Institute of Science, Bangalore 560012, India*
[b] *Laboratory of Experimental and Computational Biology, National Cancer Institute, Frederick, MD 21702-1201, USA*

Received 23 February 2000; received in revised form 1 August 2000; accepted 10 October 2000

Abstract

There is growing evidence that some enzymes catalyze reactions through the formation of short–strong hydrogen bonds as first suggested by Gerlt and Gassman. Support comes from several experimental and quantum chemical studies that include correlation energies on model systems. In the present study, the process of proton transfer between hydroxyl and imidazole groups, a model of the crucial step in the hydrolysis of RNA by the enzymes of the RNase A family, is investigated at the quantum mechanical level of density functional theory and perturbation theory at the MP2 level. The model focuses on the nature of the formation of a complex between the important residues of the protein and the hydroxyl group of the substrate. We have also investigated different configurations of the ground state that are important in the proton transfer reaction. The nature of bonding between the catalytic unit of the enzyme and the substrate in the model is investigated by Bader's atoms in molecule theory. The contributions of solvation and vibrational energies corresponding to the reactant, the transition state and the product configurations are also evaluated. Furthermore, the effect of protein environment is investigated by considering the catalytic unit surrounded by complete proteins—RNase A and Angiogenin. The results, in general, indicate the formation of a short–strong hydrogen bond and the formation of a low barrier transition state for the proton transfer model of the enzyme.

Keywords: Hydrogen bond; Proton transfer; RNA hydrolysis; Rnase A

* Corresponding author. Tel.: +91-80-3092611; fax: +91-80-3600535.
E-mail address: sv@mbu.iisc.ernet.in (S. Vishveshwara).

0301-4622/01/$ - see front matter
PII: S0301-4622(00)00221-0

1. Introduction:

A number of enzymes belong to the ribonuclease-A [1] family and catalyze the cleavage of the phosphodiester bond in RNA. Several mechanisms have been put forward to explain this catalytic process [2–6]. The crux of these mechanisms lies in the transphosphorylation step and it is here that they differ from one another. (The dinucleotide substrate in the active site pocket of RNase A is given in Fig. 1 and a schematic representation of the transphosphorylation reaction is shown in Fig. 2). Some of the proposed mechanisms are: (1) Breslow's mechanism which involves the simultaneous shift of two protons [3], (2) intra-ligand proton transfer [5], (3) short–strong hydrogen bond between the enzyme and ligand by Gerlt and Gassman [2] and (4) dianionic intermediate [6]. It should be noted that these mechanisms are not necessarily mutually exclusive and they are proposed based on different experimental and computational evidence. For instance, Breslow's mechanism of two-proton shift can very well involve short–strong hydrogen bonds, giving rise to a low barrier for proton transfer.

The proposal of short–strong hydrogen bonds (SSHB) by Gerlt and Gassman has been a source of inspiration for a number of investigations of catalytic mechanisms. The proton transfer through low barrier hydrogen bond (LBHB) [7,11] is associated with the concept of SSHB. Frey et al. have reported the likelihood of having an LBHB in the catalytic triad of serine protease [8–10]. High-level quantum chemical studies on model compounds representing the enzymatic reactions of Maleate dehydrogenase [12], enolates [13,14] and Serine protease [8] along with NMR and Pk studies have given clues to of the presence and role of short strong hydrogen bonds. The above examples are derived from different chemical systems such as Zwitterion type [8,9], globally charged system like maleate [12] and from geometrically constrained proximal donor acceptors such as enolate system [13]. We had earlier predicted such short–strong hydrogen bonds in RNA cleavage catalyzed by RNase A [15]. This is a case where the donor and the acceptor (2′-OH of ribose and imidazole of histidine) groups of the protein are neutral and unconstrained and the proton transfer between these two groups is assisted by a positively charged group (lysine).

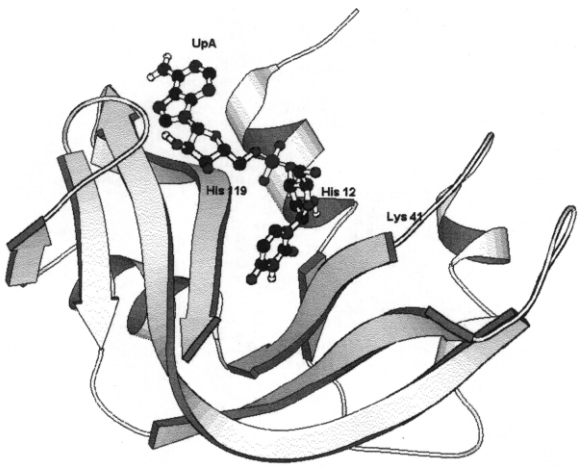

Fig. 1. Molscript [39] rendition of the dinucleotide UpA bound structure of RNase A [31].

The aim of the present investigation is to locate and characterize the transition state and also to validate our prediction [15] of the presence of SSHB in the catalytic unit of RNase A at a level of theory, which includes the correlation energy. Methanol and imidazole represent the donor and acceptor groups of the substrate and the enzyme, respectively, while the protonated methylamine represents the positively charged lysine that assists the process of proton transfer. The stability of the identified transition state is characterized by frequency analysis and the nature of bonding is investigated by Bader's atoms in molecules [16–18] formulation. Furthermore, the two minima corresponding to the configurations of the product, the reactant and the transition state along the reaction path were investigated by considering the vibrational energies and the effects of solvent. Although the catalytic process and the groups involved are the same throughout the family of RNase A like enzymes, there is a marked difference in their activity [19]. This could be due to a difference in the binding capacity or due to the effect of the environment directly on the catalytic unit. We have included the environment

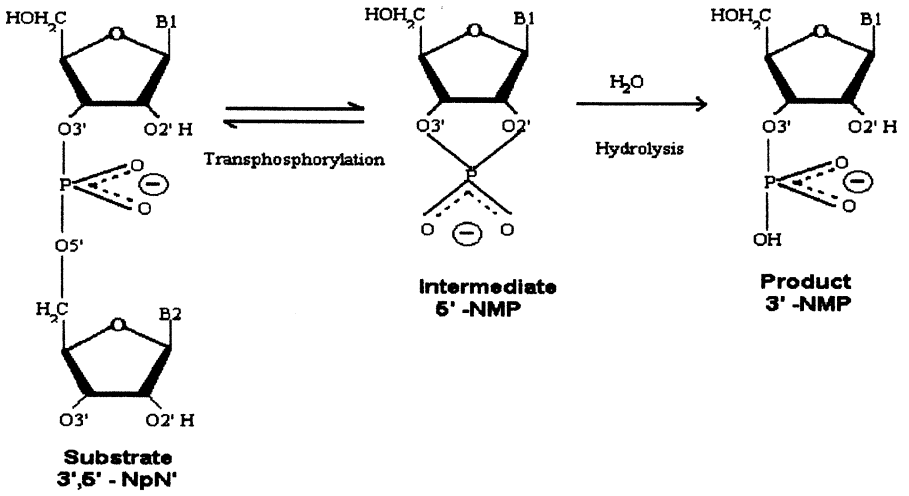

Fig. 2. A schematic representation of the catalytic mechanisms of the cleavage of the phosphodiester bond of the nucleotide by RNase A.

of the catalytic unit in the form of complete enzymes RNase A and Angiogenin (another protein catalyzing the cleavage of RNA) along with water molecules in our computations, in order to assess whether the environment has any influence on the catalytic unit.

2. Computational methods

The quantum chemical calculations were performed at different levels of theory depending on the size of the model and the level of accuracy required. The Hartree-Fock (HF) and the perturbation method at the MP2 level [20] were carried out using the 6-31 + G(d,p) basis set, which was found to be satisfactory in describing hydrogen bonded systems [21–24]. The Density Functional Theory (DFT) [25–27] based computations were carried out using B3LYP hybrid functional [28,29] and 6-31 + G(d,p) basis set. All computations were performed with the Gaussian 94 suite of pro-

Table 1
Absolute energies (in Hartree unit) and hydrogen bond energies Δe (in kcals/mol, 1 Hartree = 627.71 kcals/mol) of model systems

	Compound	Energies[a]			ΔE ($E_{complex}$–$E_{monomers}$)		
		HF	B3LYP	MP2	HF	B3LYP	MP2
1	CH_3-OH	−115.052397	−115.734871	−115.393519			
2	CH_3-NH_3 +	−95.588221	−96.228212	−95.917825			
3	Imidazole	−224.832675	−226.235384	−225.568463			
4	(CH_3-OH) imidazole	−339.894874	−341.981973	−340.975941	−6.15	−7.35	−8.76
5	(CH_3-OH)-(CH_3-NH_3) +	−210.671564	−211.996673	−211.346265	−19.42	−21.08	−21.90
6	(CH_3-OH)-imidazole-(CH_3-NH_3) +[b]	−435.532887	−438.268442	−436.953332	−37.40	−43.91	−46.14
					−31.25	−36.56	−37.38
					−17.98	−22.83	−24.22

[a]All the three levels of calculations reported in this and other tables made use of 6-31 + G(d,p) basis set unless otherwise specified.

[b]The three ΔE values for this system correspond to Emonomers = E(1) + E(2) + E(3); E(4) + E(2) and E(5) + E(3).

Table 2
Optimized bond lengths and the corresponding frequencies of the monomer, dimer and trimer complexes along with change in bond lengths (ΔBL) and frequencies (Δn) in the hydrogen bonded complexes

	Compound[a]	Bond length (Å)			Δ BL (Å)			Frequency (cm^{-1}) (Δn)
		HF	B3LYP	MP2	HF	B3LYP	MP2	B3LYP
1	CH_3-OH(O–H)	0.942	0.965	0.964				3839
2	CH_3-NH_3 + (N–H)	1.026	1.026	1.023				3401
3	CH_3-OH-IMIDAZOLE							
	(O–H)	0.950	0.979	0.977	+0.008	+0.014	+0.013	3555(−284)
	(Nh[b]...H)	3.026	2.904	2.899				
4	CH_3-OH-CH_3-NH_3(+)							
	(O–H)	0.945	0.967	0.967	+0.003	+0.002	+0.003	3825(−14)
	(Nl[c]–H)	1.028	1.065	1.053	+0.002	+0.039	+0.030	2876(−625)
	(O...Nl)	2.794	2.698	2.708				
5	CH_3-OH-IMIDAZOLE-CH_3-NH_3(+)							
	(O–H)[d]	0.966	1.028	1.020	+0. 024	+0. 063	+0.056	1960(−1869)
	(Nl–H)[d]	1.043	1.121	1.096	+0.017	+0.095	+0.073	2773(−727)
	(O...Nh)	2.818	2.637	2.640				
	(O...Nl)	2.678	2.557	2.563				

[a] The concerned bonds are enclosed in brackets.
[b] Nh is the proton acceptor atom of imidazole.
[c] Nl is the proton donor atom of CH_3-NH_3(+).
[d] The frequencies are not pure since the (O–H) and (Nl–H) motions are coupled.

grams [30]. The model systems represent the catalytic unit involved in the active site of RNase A and the mutual orientation of groups were obtained from the molecular dynamics simulation of RNase A-UpA complex [31]. The investigated model system includes the proton-donor and acceptor monomers (methanol, methylamine and imidazole) and their dimer and trimer complexes, whose starting orientations were considered from the MD simulations mentioned above. These units were investigated for their hydrogen bond strengths in different configurations that are significant in the proton-transfer path. The energies of the model systems are given in Table 1. The

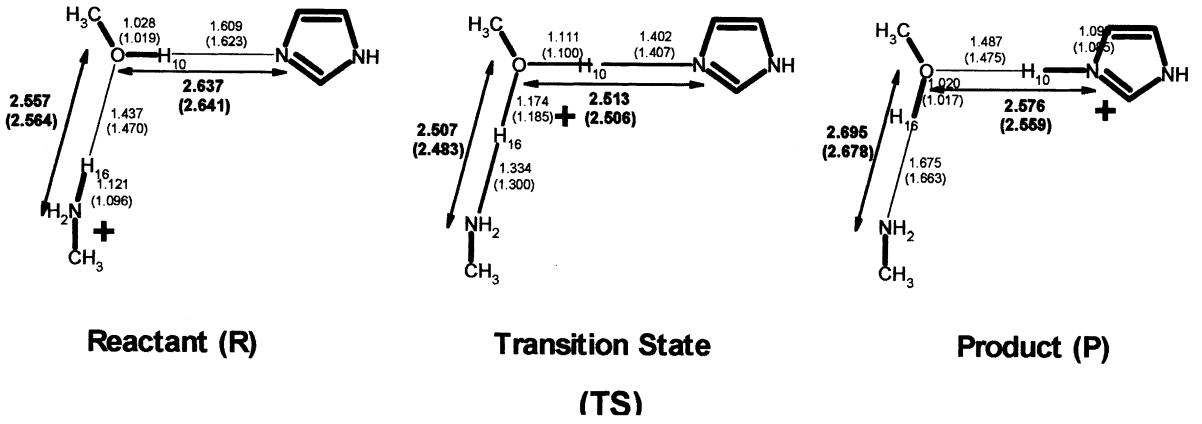

Fig. 3. The optimized bond lengths related to hydrogen bonds in the trimer complexes representing the Reactant, Transition and product States. The values reported are from DFT calculations and the numbers in parenthesis ( ) are from MP2 calculations.

results at MP2 and DFT levels are quite comparable and hence the vibrational frequency calculations were carried out only at the DFT level. The optimized geometries and the frequencies are reported in Table 2.

The proton transfer reaction was followed by optimizing the reactant (R), the product (P) and the transition state (TS) geometries, where R, P and TS represent different configurations of the ground state of the reaction complex. The three stationary configurations are henceforth denoted as P, R and TS states and were characterized by frequency analyses, with R and P states having no imaginary frequencies and the TS state with a single imaginary frequency. The optimized geometries of these configurations are presented in Fig. 3. The solvent effect on the R, P and TS states were evaluated by the Onsager- reaction field [32]. The dielectric constant values of 4, 20 and 80 were used in calculations. The relative changes in the energies of R, P and TS states due to solvent effect and zero point vibration are given in Table 4.

All three states exhibit short hydrogen bonds. In order to evaluate the nature of these bonds, a topological analysis of DFT/B3LYP/6-31 + G(d,p) electron density was performed with Bader's atom in molecule (AIM) theory. According to this theory, the topological features can be defined by the electron density [$\rho(r_c)$] at the bond critical point and the Laplacian of the electron density [$\nabla^2\rho(r_c)$] [16–18]. Generally, a bond is described as covalent involving 'shared interactions' when $\nabla^2\rho(r_c)$ is negative and $\rho(r_c)$ is large in magnitude. On the other extreme, interactions of the van der Waals and hydrogen bond types are described as 'closed shell interactions' and are characterized by a relatively low value of $\rho(r_c)$ and a positive value of $\nabla^2\rho(r_c)$. These indicators however should cautiously be used to assess the nature of bonding in a given molecular environment. [33]. In the present case, the qualitative inferences drawn from this study are meaningful since the bonding nature and relative strengths of similar systems (R, P and TS states) have been compared

We have also made an attempt to assess whether the enzyme environment has any effect on the energetics of the catalytic process. A more realistic catalytic system with ribose phosphate, two imidazole rings and protonated methylamine was chosen for this investigation [Fig. 4a]. The ribose phosphate model includes the proton donor 2′-OH in a five membered pyranose ring and the phosphate group which is catalytically cleaved by the enzyme is on the 3′-OH of ribose. Imidazole (1) represents histidine-12 that accepts a proton from 2′-OH and imidazole (2) represents histidine 119 of RNase A that donates a proton to the phosphate group. The protonated methylamine represents Lysine 41, which assists in proton transfer to imidazole (1). This system of 49 atoms (catalytic unit), the geometry of which was obtained from MD simulation of RNase A-UpA complex [31] was optimized HF/ 3-21G level. The optimized geometry was then superimposed back on to the relevant atoms of the RNase A-UpA complex. This optimized catalytic unit was also superimposed on the coordinates obtained from the MD simulation of the modeled Angiogenin-nucleotide complex [34], which retains an active site similar to that of RNase A. A layer of water molecules surrounded both enzymes. The net atomic charges on all the atoms of the protein and the nucleotide were obtained from AMBER force field [35,36] and TIP3P [37] charges were used on the water molecules. After superimposing the catalytic unit on to the two solvated enzyme systems, the atoms making short contact (<2 Å) were eliminated. The following three environments were created from RNase A and Angiogenin by including point charges on the protein and water atoms: (1) all atoms within a cutoff radius of 12 Å (Fig. 4b); (2) all atoms of the protein (Fig. 4c); and (3) all protein and water atoms in the complete box (Fig. 4d). Single point calculations at HF/3-21G level were carried out on these systems. Electrostatic properties such as net atomic charges (Mulliken and Merz-Kollman) and the dipole moment of the catalytic unit were analyzed. The results show a considerable variation in these properties as a function of the environment as shown in Table 5 and will be discussed in the results section.

3. Results and discussion:

The first step in the catalysis of RNA cleavage involves the transfer of a proton from the 2′ hydroxyl group of the ribose to the imidazole of Histidine in the presence of Lysine (Fig. 2). Methanol, imidazole and protonated methylamine groups were chosen as model compounds to represent ribose, histidine and lysine, respectively. The energies and the geometries of the model monomers, relevant dimers and trimers representing the active site complex are discussed in section 1. The topologies and the energies (including solvent and vibrational contributions) of the trimer complexes of R, P and TS states are discussed in section 2. Finally, the results on an extended model with protein environment are discussed in section 3.

3.1. Model compounds

The energies of the model monomers along with the relevant dimer and trimer complexes are evaluated at the HF and at the MP2 level of perturbation theory. A uniform basis set of 6-31 + G(d,p) was used in these sets of calculations. The DFT calculations were carried out using the B3LYP functional. Our earlier optimizations were carried out at the HF/(3-21G) level [15] in which we observed a short hydrogen bond between methanol and imidazole when protonated methylamine was hydrogen bonded to the hydroxyl

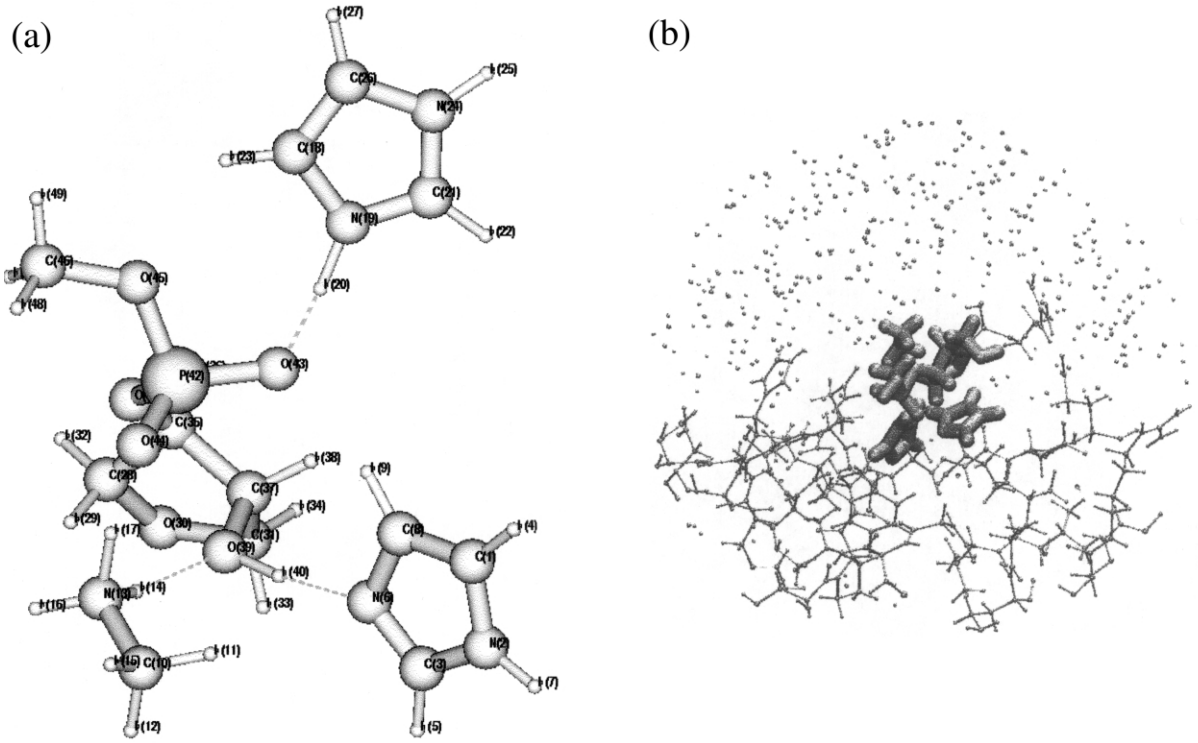

Fig. 4. (a) A ball and stick representation of the 49 atom catalytic unit drawn using MOLDEN (G. Schaftenaar, MOLDEN, 1991). The two dotted lines corresponding to the hydrogen bonds of the 2′-OH group of the ribose with the imidizole group of Histidine 12 and the amino group of Lysine 41. The third dotted line represents the hydrogen bond between the imidazole group of Histidine 119 and the phosphate oxygen. (b) The catalytic unit in (a) is surrounded by the protein (Angiogenin [34]) and water molecules present within a radial distance of 12Å. (c) The catalytic unit in (a) is surrounded by all atoms of the protein (Angiogenin). (d) The catalytic unit in (a) is surrounded by all atoms of the protein as well water molecules of the simulation box [34].

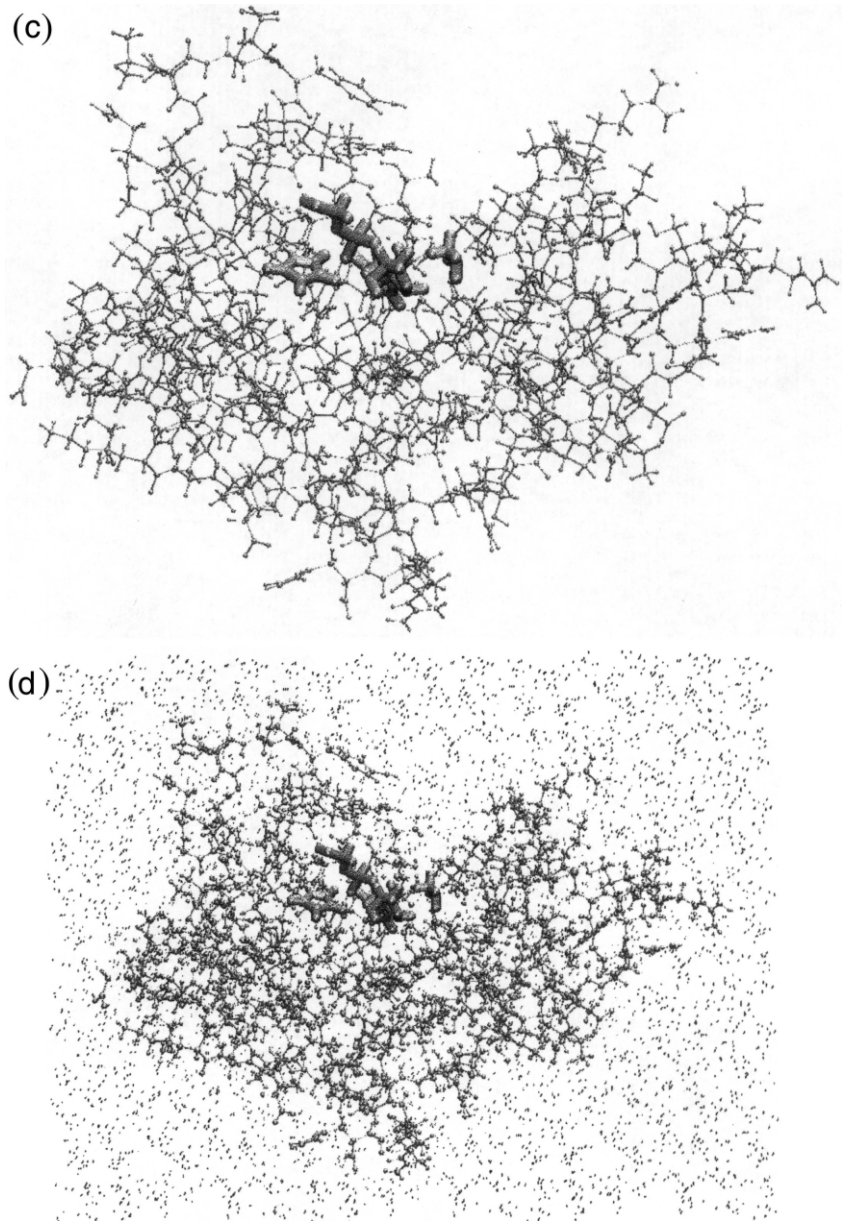

Fig. 4. (*Continued*)

group of methanol (R state). This level of theory, however, was unable to detect stable TS and P states. More accurate estimates of the energies and the geometries are obtained at the DFT and MP2 levels and the results are compared with those obtained from HF/(6-31 + G(d,p)) in Tables 1 and 2. The presence of strong hydrogen bonds in the dimer with protonated methylamine, and in the trimer is consistently represented at all three levels of theory. The evaluated hydrogen bond energies are lowest at the HF level and highest at the MP2 level and the DFT energies

are very close to that at the MP2 level. Perceptible differences are seen in the optimized hydrogen bond lengths and the lengths of covalent bonds (O–H or N–H) involved in the hydrogen bond in the HF, DFT and MP2 levels. The predicted hydrogen bonds are shorter and the covalent bonds involving the proton donors are longer as evaluated at the DFT and MP2 levels when compared to those evaluated at the HF level. This trend is particularly enhanced in the trimer complex where the optimized O…N (imidazole) hydrogen bond length is 2.82 Å at the HF level and 2.64 Å at the DFT and MP2 levels. Similarly, the O…N (Lysine) lengths are 2.68 Å at the HF level and 2.56 Å at the DFT and MP2 levels. It is known that the IR stretching frequencies of covalent bonds are modified in hydrogen bonded complexes [21–24] and this is apparent from the values given in Table 2. The reduction in the frequencies of the vibration involved in hydrogen bonds in the trimer complex is significantly higher than in the dimer complexes. Although the reduction in the IR frequency in the trimer complex cannot be quantitatively correlated with the hydrogen bond strength, it is qualitatively consistent with the short–strong hydrogen bond.

3.2. The proton transfer reaction

In order to follow the proton transfer reaction, the proton of methanol in the trimer complex (R-state) was shifted to the covalent bond position with the nitrogen of imidazole to obtain the P state. The TS state, where the methanol proton is in between the two electronegative atoms was located as a transition state by providing the optimized R and P states as input. The P and TS states stabilized to their respective states during optimization at the DFT and MP2 levels, unlike in the case of HF/3-21G optimization [15]. This emphasizes the importance of the correlation energy in hydrogen bonds, particularly in short hydrogen bonds.

The geometries of the three states optimized at the DFT and MP2 levels are presented in Fig. 3. The oxygen atom (corresponding to 2′-OH) is simultaneously involved in two hydrogen bonds. It acts as a proton donor to imidazole and acceptor from methylamine in the R state and vice versa in the P state. Both hydrogen bonds are short compared to normal neutral hydrogen bonds. It should be noted that in the R and P states, the hydrogen bond with oxygen as the proton donor is slightly longer than the other hydrogen bond in which the oxygen atom is the proton acceptor. The TS state exhibits a very interesting geometry. Both hydrogen bonds in this state are shorter than the hydrogen bonds in the R and P states and both protons are close to the oxygen atom. This indicates a shift of the net positive charge on to the oxygen atom as opposed to that on the nitrogen atoms in the R and P states. The O–H bonds are however slightly longer as would be expected of a very short hydrogen bond.

The bonding characteristics in the three optimized states were further analyzed by frequency analysis at the DFT/B3LYP level. The R and the P states were clearly established as minima with no imaginary frequencies. The TS state however, had a single imaginary frequency, which confirmed that it was a transition state. The normal modes of this frequency exhibited a large displacement in the positions of the protons H10 and H16 (Fig. 3), indicating that the reaction path considered indeed involves the transfer of these two protons. The frequencies corresponding to the stretch of O–H and N–H bonds involved in the hydrogen bonds were identified and found to be significantly reduced. The frequency reductions were consistent with the bonds involved in hydrogen bond formation in a given state, with the TS state exhibiting a drastic reduction in both the O–H and N–H stretch. This indicates a correlation of the strength of the hydrogen bond with the vibrational frequency in these systems.

An estimate of the nature of the bond can be obtained by Bader's atoms in molecules (AIM) analysis [16–18] and the results of such an analysis on the R, P and TS states at DFT/B3LYP level are presented in Table 3. A good correlation is seen between the electron density and the bond length between two atoms. The electron density is the lowest (0.06) in the longest bond (1.675 Å) and is highest (0.30) in the shortest bond (1.020 Å) of the P state. It is interesting to note that the Laplacian of the electron density is negative for

Table 3
Charge density [$\rho(r_c)$] [in $(e/a_0{}^3)$], Laplacian of the charge density $\nabla^2\rho(r_c)$ [in $(e/a_0{}^5)$] and bond length (bl) [in A^0] of the bonds involved in proton transfer in the three states (R, TS and P)

Bond[a]	Reactant (R) $\nabla^2\rho(r_c)$, [$\rho(r_c)$], (bl)	Transition State (TS) $\nabla^2\rho(r_c)$, [$\rho(r_c)$], (bl)	Product (P) $\nabla^2\rho(r_c)$, [$\rho(r_c)$], (bl)
CH_3OH----$N^{imidazole}$	+1.11 [0.07] (1.609)	−0.05 [0.12] (1.402)	−1.35 [0.27] (1.090)
CH_3O—H	−1.49 [0.29] (1.028)	−0.84 [0.22] (1.112)	+0.16 [0.08] (1.488)
(CH_3)-(HO)----H-(NH_2CH_3) +	+0.14 [0.09] (1.437)	−0.55 [0.19] (1.174)	−1.57 [0.30] (1.020)
(CH_3)-$(H_2N$—H) +	−1.20 [0.25] (1.121)	−0.23 [0.14] (1.334)	+0.10 [0.06] (1.675)

[a] The long solid and broken lines correspond to covalent and hydrogen bonds, respectively, in the P state and the reported values correspond to these bonds in the three states.

all the four bonds in the TS state, indicating a covalent nature of these bonds in the transition state. The Laplacian of the electron density corresponding to two hydrogen bonds in the R and the P states are positive as expected. Earlier, AIM calculations demonstrated transition states with covalent character in geometrically constrained systems of maleate [12] and enolate [13]. And here, for the first time, we have shown the possibility of a transition state complex with a strong bond in an unconstrained system.

Finally, the energetics of different configurations along the reaction path is investigated by evaluating other components to the energies at DFT/B3LYP level. More specifically, a modification of the electronic energy by the vibrational component and by solvent effect is carried out and the results are consolidated in Table 4. The difference in energies (energies in kcal/mol are given in parentheses) are evaluated with respect to the R state. Negative values for the P state at all levels indicate that the P state is probably the global minimum in the reaction pathway. The electronic energy at both the DFT/B3LYP and

Table 4
Energies of the three optimized structures (R, TS and P) along with the vibrational and the solvent contributions

Energies (in atomic units)	R	TS	P
Electronic (E_0)			
E_0 (MP2/)	−436.95333	−436.950 38(+1.85)[a]	−436.95380 (−0.31)
E_0 (DFT/B3LYP)	−438.26844 [5.76][b]	−438.26675 (+1.07) [2.29]	−438.27137 (−1.84) [3.90]
Solvent[c]			
$E_0 + E_{solvent}$			
Dielectric constant = 4	−438.27177 [6.48]	−438.26722 (+2.85) [2.55]	−438.27245 (−0.43) [4.46]
Dielectric constant = 20	−438.27337 [6.81]	−438.26747 (+3.70) [2.67]	−438.27369 (−0.20) [4.67]
Dielectric constant = 80	−438.27373 [6.89]	−438.26753 (+3.89) [2.69]	−438.27385 (−0.08) [4.72]
Vibrational[c]			
$E_0 + E_{\text{zero point}}$	−438.06407	−438.06781 (−2.35)	−438.06764 (−2.23)
$E_0 + E_{\text{Gibbs free energy}}$	−438.10818	−438.11016 (−1.24)	−438.11065 (−1.55)

[a] The energy values are in Hartree units and the values in bracket ( ) are the ΔE (kcal/mol) with respect to the reactant at the chosen level of calculation.

[b] The values in square bracket [ ] are the Dipole moments [debye].

[c] Solvent and vibrational energies are at the DFT/B3LYP level.

MP2 levels indicate a small barrier for the TS state. The effect of solvent is to increase the barrier by increasing the energy difference between the R and the TS states. The solvent effect is a function of dielectric constant, with an increase in the barrier with increase in the dielectric constant. This feature is related to the dipole moment of the model system. The evaluated dipole moments are highest for the R state and least for the TS. The zero point vibration and the Gibbs free energy on the other hand facilitates the reaction by lowering the energy of the TS even below the R state. Thus the proton transfer reaction catalyzed by the RNase A family of proteins seems to proceed not only through short strong hydrogen bonds, but also through a low barrier hydrogen bond (LBHB) mechanism. The point to emphasize is that the LBHB arises due to an increase in the covalent character and the vibrational free energy contributions to the transition state.

3.3. Effect of protein environment

From the above studies, it appears that a delicate balance of various components drives the catalytic reaction in the right direction. Although the immediate catalytic environment is the same in all the RNase A family proteins, the activities on the same substrate differs from protein to protein. One reason can be a difference in the exact mode of binding and secondly the protein environment can affect the energetics of the catalytic reaction. In order to probe the second possibility, we have recreated different enzyme environment and investigated its effect on the active site model. The details of the construction of the catalytic unit (Fig. 4a) and its environment have been described in the method section. The protein and the atoms of the water molecules are treated as point charges and the effect of these charges on the catalytic unit is evaluated in terms of the change in the dipole moment. The change in the dipole moment of small molecules due to solvation has been documented experimentally and computationally [38] and hence it is logical to expect changes in the electrostatic properties of the catalytic unit due to the effect of the protein environment.

Three different environments (Fig. 4a,b,c) were used both in the case of Rnase A and angiogenin. Qualitative changes were not seen in the net atomic charges evaluated by Mulliken and Merz-Kollman methods and hence only the Mulliken charges and dipole moments are reported in Table 5. Different environments, however, had a pronounced effect on the dipole moment of the catalytic unit, which can influence the solvation energy considerably as we have seen earlier. The net charge in the environment has a considerable influence on the dipole moment of the catalytic unit. In Angiogenin, a net charge of $+0.8$ electronic charges is provided by the 12 Å cutoff and close to $+13$ units in the full protein and protein + water environment (Angiogenin contains 16 acidic and 29 basic groups). The dipole moment in the 12 Å cutoff environment is very close to that of the isolated catalytic unit, whereas it is significantly higher in the other two cases for which the net charges are high. RNase A provides -4.2 electron units at 12 Å cutoff and $+5.0$ units with the full protein and protein + water environment (RNase A contains 9 acidic and 14 basic groups). The dipole moment of the catalytic unit is considerably higher in all these three cases. The change in the dipole moment is due to a change in the net atomic charges. Some of the changes in the net atomic charges on catalytically important atoms are significant as shown in Table 5. Thus it appears that the protein environment in terms of its net charge and the spatial distribution of charges can have significant influence on the electrostatic properties of the catalytic unit, which in turn can give rise to differences in the contribution from the environment. In other words, a reaction may become possible in the enzyme environment which otherwise may not take place even if the crucial residues are placed in the appropriate orientation in the absence of a proper environment.

3.4. Summary

Quantum chemical calculations at the perturbation theory level of MP2 and density functional

Table 5
Variation of net atomic charges (Mulliken) of the atoms involved in proton transfer and dipole moment of the system with environment

Angiogenin	Angiogenin			
	Vacuum	12A Radial cut-off	Only protein	Full environment
No. of atoms in environment	–	943	2006	11450
Net charge of environment	–	0.8	12.8	12.8
Dipole moment(debyes)	9.4	9.7	15.6	17.6
Atomic[a] charge				
N6	−0.769	0.769	0.700	−0.699
O39	−0.783	0.784	−0.773	−0.771
H40	0.482	0.482	0.460	0.463
N13	−0.950	0.949	0.779	−0.778
H14	0.462	0.462	0.413	0.405
N19	−0.928	0.930	−0.878	−0.744
H20	0.546	0.546	0.570	0.615
O43	−0.954	0.953	−0.910	−0.919
	RNase A			
	Vacuum	12A Radial cut-off	Only protein	Full environment
No. of Atoms in environment	–	1157	1764	8698
Net charge of environment	–	−4.2	5.0	5.0
Dipole moment(debyes)	9.4	12.9	16.3	15.4
Atomic charge				
N6	−0.769	−0.598	−0.641	−0.641
O39	−0.783	−0.684	−0.702	−0.699
H40	0.482	0.472	0.463	0.464
N13	−0.950	−1.030	−1.007	−1.029
H14	0.462	0.510	0.534	0.532
N19	−0.928	−1.001	−0.994	−1.005
H20	0.546	0.553	0.553	0.545
O43	−0.954	−0.890	−0.862	−0.856

[a]Atom numbers are as in Fig. 4a.

theory are carried out on the catalytic unit of RNase A. Methanol, imidazole and protonated methyl-amine are used as model compounds to represent the proton donor 2′-OH of the ribose of RNA, the proton acceptor histidine 12 and the catalysis assisting residue lysine 41 of Rnase A, respectively. Ground state configurations of the reactant (R), product (P) and the transition state (TS) are considered along the proton transfer reaction path. The following results are obtained on these three states.

The optimization leads the R and the P states to minima and the TS to a transition state as seen by the frequency analysis. The optimized geometries indicate short strong hydrogen bonds (SSHB) between the 2′-OH group of ribose (methanol) and the imidazole nitrogen corresponding to histidine 12 of RNase A, with the O……N bond distance being 2.64 Å, 2.50 Å and 2.56 Å, respectively, in the R, TS and the P states. This SSHB between the neutral proton donor and the acceptor is assisted by simultaneous hydrogen bond formation of the donor with the positively charged lysine 41 (nitrogen of protonated methylamine).

Bader's atoms in molecule calculations of the Laplacian of the electron density also supports the view that the TS state is stabilized by simultaneous formation of a strong bond between the bridging proton and the electronegative atoms of proton donor and acceptor

The SSHB between the enzyme–substrate model in the R, TS and the P states also results in a low barrier for proton transfer (LBHB), with the P state being the energy minimum. The electronic energies of the three states are modified by vibrational and solvent contributions to different extents. The TS state is stabilized by the vibrational energy and destabilized by the solvation energy with respect to the R state. The solvent effects are correlated with the net dipole moment of the system and the protein environment influences the energetics of the catalytic unit by affecting its dipole moment. The effect of the environment on the dipole moment has been demonstrated by using the enzyme environment of Rnase A family proteins–RNase A and Angiogenin. This result may have implication on the differences in the activities of the two enzymes.

Acknowledgements

S. Vishveshwara wishes to thank the National Cancer Institute for a visiting position. We thank the Super Computer Education and Research Centre of the Indian Institute of Science and the Advanced Biomedical Computing Center, Frederick for computational facilities. Support from the Department of Science and Technology [grant no SP/SO/D-107/98 to S.V.], India is also acknowledged.

References

[1] J.J. Beintema, J.H. Breukelman, A. Carsana, A. Furia, Ribonucleases; structures and functionsAcademic Press, 1997, pp. 245–269.
[2] J. Gerlt, P.G. Gassman, Biochemistry 32 (1993) 11943–11952.
[3] R. Breslow, R. Xu, Proc. Natl. Acad. Sci. USA 90 (1993) 1201.
[4] D.J. Herschlag, Am. Chem. Soc. 116 (1994) 11631.
[5] C. Lim, P. Tole, J. Am. Chem. Soc. 114 (1992) 7245.
[6] M.T. Glenon, A. Warshel, J. Am. Chem. Soc. 120 (1998) 10234–10247.
[7] W.W. Cleland, M.M. Kreevoy, Science 264 (1994) 1887–1890.
[8] P.A. Frey, S.A. Whitt, J.B. Tobin, Science 264 (1994) 1927–1930.
[9] J.B. Tobin, S.A. Whitt, C.S. Cassidy, P.A. Frey, Biochemistry 34 (1995) 6919–6924.
[10] C.S. Cassidy, J. Lin, P.A. Frey, Biochemistry 36 (1997) 4576–4584.
[11] W.W. Cleland, M.M. Kreevoy, P.A. Frey, Science 269 (1995) 104–106.
[12] M. Garcia-Viloca, A. Gonzalez-Lafont, J.M. Lluch, J. Phys. Chem. A 101 (1997) 3880–3886.
[13] B. Schøit, B.B. Iversen, G.K.H. Madsen, F.K. Larsen, T.C. Bruice, Proc. Natl. Acad. Sci. U.S.A. 95 (1998) 12799–12802.
[14] B. Schøit, B.B. Iversen, G.K.H. Madsen, T.C. Bruice, J. Am. Chem. Soc. 120 (1998) 12117–12124.
[15] S. Vishveshwara, R. Jacob, G. Nadig, J.V. Maizel Jr., J. Mol. Str. 471 (1998) 1–11.
[16] R.F.W. Bader, Atoms in molecules: a quantum theory-Oxford Univ Press, London, 1990.
[17] R.F.W. Bader, S. Johnson, T.-H. Tang, P.L.A. Popelier, J. Phys. Chem. 100 (1996) 15398–15415.
[18] R.F.W. Bader, Chem. Rev. 91 (1991) 593–928.
[19] J.F. Riordan, Ribonucleases structures and functionsAcademic press, New York, 1997, pp. 445–489.
[20] C. Moller, M.S. Plesset, Phys. Rev. 46 (1934) 618.
[21] K. Kim, K.D. Jordan, J. Phys. Chem. 98 (1994) 100089.
[22] J.J. Nova, C. Sosa, J. Phys. Chem. 99 (1995) 15837.
[23] J.E. Del Bene, J. E. hydrogen bonding: 1 encyclopedia of computational chemistry. John Wiley and Sons 2 (1998) 1263–1271.
[24] M. Hartmann, L. Radom, J. Phys. Chem. 104 (2000) 968–973.
[25] P. Hohenberg, W. Kohn, Phys. Rev. 136 (1964) 864.
[26] W. Kohn, I.J. Sham, Phys. Rev. A 140 (1965) 1133.
[27] B.G. Johnson, P.M.W. Gill, J.A. Pople, J. Chem. Phys. 98 (1993) 5612–5626.
[28] A.D. Becke, J. Chem. Phys. 98 (1993) 5648.
[29] C. Lee, W. Young, R.G. Parr, Phys. Rev. B 37 (1988) 1324.
[30] M.J. Frisch, G.W. Trucks, H.B Schlegel, et al., Gaussian 94, Gaussian, Inc, Pittsburgh, PA, 1995.
[31] G. Nadig, S. Vishveshwara, Biopolymers 42 (1997) 505–519.
[32] L. Onsager, J. Am. Chem. Soc. 58 (1938) 1486.
[33] R.F.W. Bader, H.J. Essen, J. Chem. Phys. 80 (1984) 1943.

[34] M.S. Madhusudhan, S. Vishveshwara, Curr. Sci. 78 (2000) 852–857.
[35] D.A. Pearlman, D.A. Case, J.W. Caldwell et al., Amber 4.1, University of California, San Francisco, 1995.
[36] W.D. Cornell, P. Cieplak, C.I. Bayly et al., J. Am. Chem. Soc. 117 (1995) 5179–5197.
[37] W.L. Jorgensen, J. Chandrashekar, J.D. Madura, R.W. Impey, M.L. Klien, J. Chem. Phys. 79 (1983) 926–935.
[38] C.J. Cramer, D.G. Truhlar, Chem. Rev. 99 (1999) 2161–2200.
[39] P.J. Kraulis, J. Appl. Crystallogr. 24 (1991) 946–950.